Available online at www.sciencedirect.com
ScienceDirect
Comput. Methods Appl. Mech. Engrg. 278 (2014) 1–19
Computer methods in applied mechanics and engineering
www.elsevier.com/locate/cma

An accurate error estimator for Guyan reduction

Jin-Gyun Kim, Phill-Seung Lee*

Division of Ocean Systems Engineering, Korea Advanced Institute of Science and Technology, 291 Daehak-ro, Yuseong-gu, Daejeon 305-701, Republic of Korea

Received 25 February 2014; received in revised form 2 May 2014; accepted 4 May 2014
Available online 10 May 2014

Highlights

- We propose an accurate error estimator for Guyan reduction.
- The error estimator can estimate relative eigenvalue errors in reduced models.
- We present the excellent performance through various numerical examples.

Abstract

The objective of this study is to develop an error estimator that accurately predicts relative eigenvalue errors in finite element models reduced by Guyan reduction. We present a derivation procedure for the error estimator, in which Kidder's transformation matrix for Guyan reduction is employed. We demonstrate the excellent performance of the proposed error estimator through various numerical examples: rectangular plate, cylindrical panel, hyperboloid panel, and shaft–shaft interaction problems.

Keywords: Eigenvalue problem; Structural dynamics; Finite element method; Model reduction; Guyan reduction; Error estimation

1. Introduction

Due to the rapidly increasing size of finite element models in engineering practice, reduced-order modeling techniques are becoming increasingly important in computational mechanics. In the 1960s, Guyan proposed a DOFs (degrees of freedom) based reduction method [1]. At the same time, similar methods were introduced by Irons [2,3]. These methods are generally referred to as Guyan reduction (sometimes also referred to as Irons–Guyan reduction, eigenvalue economizer, mass condensation, and dynamic condensation). Since then, various DOFs based reduction methods have been proposed [4–7]. Recently, related studies have focused on efficient iterative procedures to improve the level of accuracy [8–13] or on combinations with substructuring approaches for better computational efficiency [14–17].

In the DOFs based reduction method, a small proportion of the dominant DOFs, known as "master", is only retained in the reduced model, and the remaining DOFs, known as "slave", are eliminated. Therefore, the size of the original model can be significantly reduced. The accuracy of the reduced model highly depends on the choice of master DOFs. Thus, a proper selection of the master DOFs is very important, and much effort has gone into the creation

* Corresponding author. Tel.: +82 42 350 1512; fax: +82 42 350 1510.
E-mail address: phillseung@kaist.edu (P.S. Lee).

http://dx.doi.org/10.1016/j.cma.2014.05.002
0045-7825/

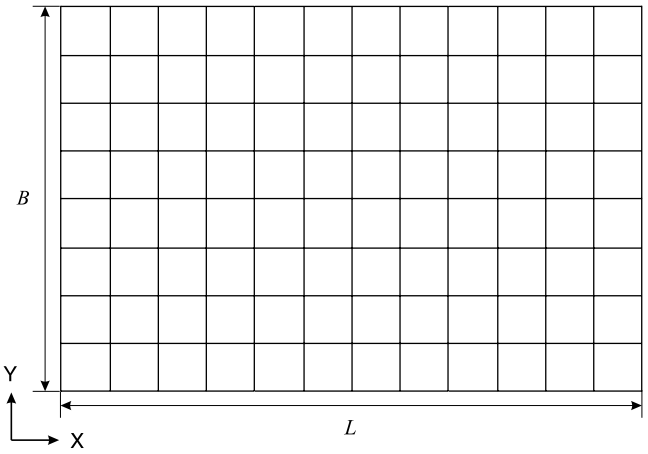

Fig. 1. Rectangular plate problem ($L = 3$ m, $B = 2$ m, $h = 0.008$ m, $E = 69$ GPa, $\upsilon = 0.35$ and $\rho_s = 2700$ kg/m^3).

of DOFs selection methods [18–22]. Similarly, in mode based methods like component mode synthesis and modal transformation methods, the selection of modes is also a key issue [23–25].

However, there has not been a good methodology to estimate the reliability of the reduced model. In particular, a method to estimate the relative eigenvalue errors in reduced models is needed but no such method exists. Therefore, the usefulness of the DOFs based reduction methods has been limited. This is a major drawback associated with DOFs based reduction methods. This fact is well revealed by Hughes's statement [26]: "A disadvantage of reduction techniques such as the Irons–Guyan procedure is that there is no guarantee that the eigenvalues and eigenvectors of the reduced problem will be good approximations of those of the original problem". This difficulty could be indirectly avoided by using some iterative procedures [9,10,12].

The objective of this study is to develop an error estimator that accurately predicts relative eigenvalue errors in finite element models reduced by Guyan reduction without using any iterative procedure. Basically, it is not easy to estimate relative eigenvalue errors because the exact eigenvalues of the original model are unknown. To derive the error estimator, the original exact eigenvector is decomposed into the approximated and error parts and Kidder's transformation matrix is used to approximate the exact eigenvector [4]. The decomposed eigenvector and Kidder's transformation matrix are substituted into the original eigenvalue problem and, analyzing the resulting expanded terms, the error estimator is obtained. The derivation procedure is simple and straightforward. In particular, the required computational cost is low because only simple additions and multiplications of known matrices are necessary.

In order to test the feasibility and performance of the proposed error estimator, we calculate both the exact relative eigenvalue errors and the estimated errors using the proposed error estimator, after which the error values are compared. Various numerical examples are considered for performance tests: rectangular plate, cylindrical panel, hyperboloid panel, and shaft–shaft interaction problems.

In the following sections, we review Guyan reduction, derive the proposed error estimator, demonstrate the performance of the error estimator, and provide conclusions.

2. Guyan reduction

In this section, we introduce the general framework of the DOFs based reduction methods, the original formulation of Guyan reduction [1] and Kidder's transformation matrix [4].

2.1. General framework

The eigenvalue problem of the original model is

$$\mathbf{K}(\boldsymbol{\varphi})_i = \lambda_i \mathbf{M}(\boldsymbol{\varphi})_i, \quad i = 1, 2, \ldots, N, \text{ with } \mathbf{u} = \boldsymbol{\Phi}\mathbf{q}, \tag{1}$$

where $\mathbf{M}$ and $\mathbf{K}$ are the mass and stiffness matrices of the original model, respectively, and λ_i and $(\boldsymbol{\varphi})_i$ are the original eigenvalue and eigenvector, respectively. N is the number of DOFs in the original model, and $\boldsymbol{\Phi}$ and $\mathbf{q}$ are the original eigenvector matrix and generalized coordinate vector, respectively.

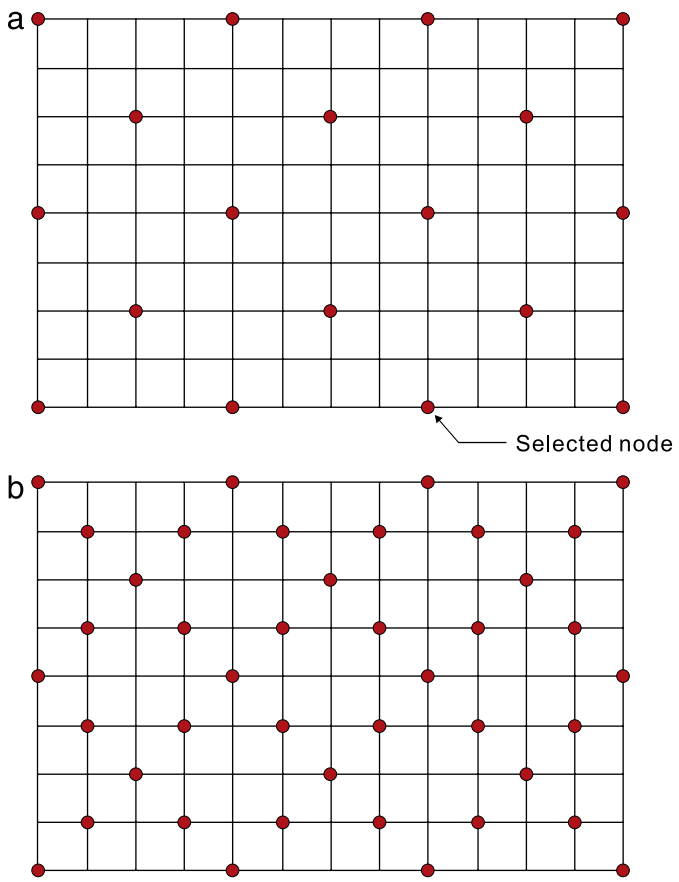

Fig. 2. Selected nodes in the rectangular plate problem. (a) 18 nodes and (b) 42 nodes. At each selected node, all DOFs are considered as master DOFs.

Table 1
Exact and estimated eigenvalue errors in the rectangular plate problem.

Mode number	(a) Case of 18 nodes selected		(b) Case of 42 nodes selected	
	Exact	Estimated	Exact	Estimated
1	4.04931E−03	4.06570E−03	6.12028E−05	6.12065E−05
2	4.54842E−03	4.56911E−03	4.09478E−05	4.09497E−05
3	2.15568E−02	2.20182E−02	3.82729E−04	3.82895E−04
4	2.35866E−02	2.41398E−02	2.15964E−04	2.16007E−04
5	3.26772E−02	3.37287E−02	2.95202E−04	2.95279E−04
6	4.18417E−02	4.35635E−02	7.44680E−04	7.45259E−04
7	6.74957E−02	7.15778E−02	1.38201E−03	1.38409E−03
8	7.98171E−02	8.46410E−02	1.62173E−03	1.62523E−03
9	1.28520E−01	1.45496E−01	1.67370E−03	1.67619E−03

The eigensolutions λ_i and $(\boldsymbol{\varphi})_i$ satisfy the following relations

$$(\boldsymbol{\varphi})_i^T \mathbf{M} (\boldsymbol{\varphi})_j = \delta_{ij} \quad \text{for } i \text{ and } j = 1, 2, \ldots, N, \tag{2a}$$

$$(\boldsymbol{\varphi})_i^T \mathbf{K} (\boldsymbol{\varphi})_j = \lambda_j \delta_{ij} \quad \text{for } i \text{ and } j = 1, 2, \ldots, N, \tag{2b}$$

where δ_{ij} is the Kronecker delta ($\delta_{ij} = 1$ if $i = j$, otherwise $\delta_{ij} = 0$). Eqs. (2a) and (2b) are called "mass-orthonormality" and "stiffness-orthogonality", respectively.

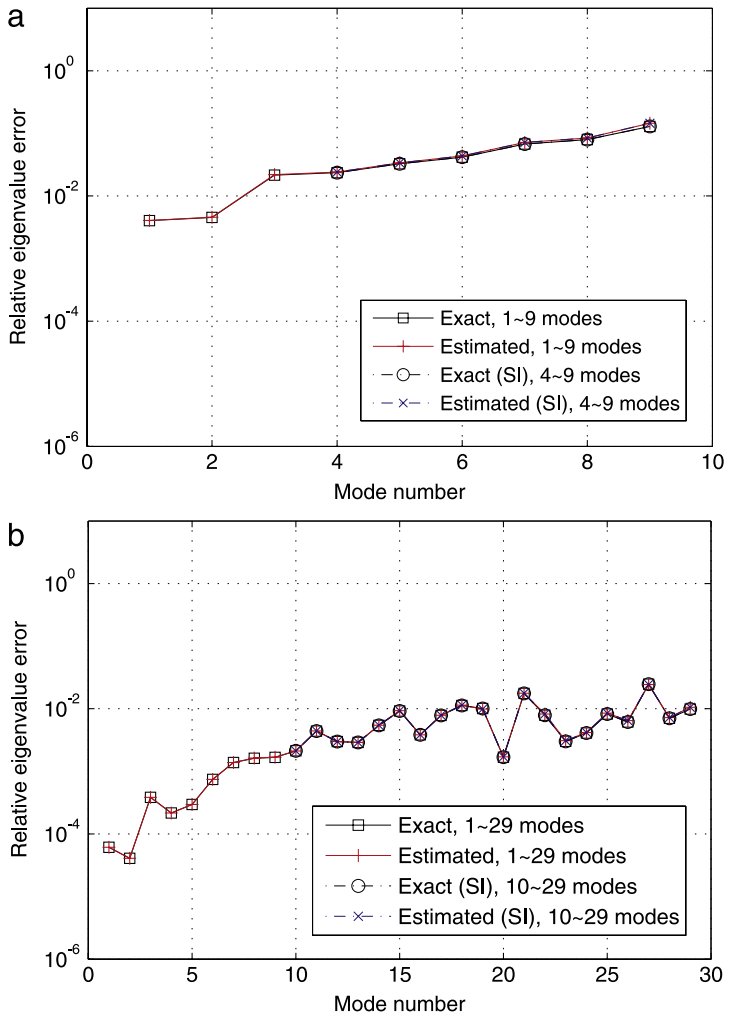

Fig. 3. Exact and estimated relative eigenvalue errors in the rectangular plate problem. (a) 18 nodes and (b) 42 nodes.

In the DOFs based reduction method, we retain the dominant DOFs and the others are eliminated. Irons named these as "master" and "slave" DOFs [2,3], which are denoted here using subscripts 1 and 2, respectively. After eliminating the slave DOFs, a reduced eigenvalue problem with only master DOFs is obtained

$$\mathbf{K}_1(\boldsymbol{\varphi}_1)_i = \bar{\lambda}_i \mathbf{M}_1(\boldsymbol{\varphi}_1)_i, \quad i = 1, 2, \ldots, N_1, \text{ with } \mathbf{u}_1 = \boldsymbol{\Phi}_1 \mathbf{q}_1, \tag{3a}$$

$$\mathbf{M}_1 = \mathbf{T}^T \mathbf{M} \mathbf{T}, \qquad \mathbf{K}_1 = \mathbf{T}^T \mathbf{K} \mathbf{T}, \tag{3b}$$

in which $\bar{\lambda}_i$ and $(\boldsymbol{\varphi}_1)_i$ are the eigenvalue and eigenvector obtained from the reduced mass and stiffness matrices denoted by $\mathbf{M}_1$ and $\mathbf{K}_1$, respectively. Here, $\mathbf{M}_1$ and $\mathbf{K}_1$ can be defined by the transformation matrix $\mathbf{T}$ constructed by eliminating the slave DOFs. N_1 is the number of DOFs in the reduced model, which is much smaller than N ($N_1 \ll N$), and the reduced displacement vector $\mathbf{u}_1$ can be expressed by the reduced eigenvector matrix $\boldsymbol{\Phi}_1$ and its generalized coordinate vector $\mathbf{q}_1$. Note that an overbar $\overline{(\cdot)}$ denotes approximated quantities.

In Eq. (3), $\bar{\lambda}_i$ and $(\boldsymbol{\varphi}_1)_i$ also satisfy the mass-orthonormality and stiffness-orthogonality conditions with the reduced mass and stiffness matrices:

$$(\boldsymbol{\varphi}_1)_i^T \mathbf{M}_1 (\boldsymbol{\varphi}_1)_j = \delta_{ij} \quad \text{for } i \text{ and } j = 1, 2, \ldots, N_1, \tag{4a}$$

$$(\boldsymbol{\varphi}_1)_i^T \mathbf{K}_1 (\boldsymbol{\varphi}_1)_j = \bar{\lambda}_j \delta_{ij} \quad \text{for } i \text{ and } j = 1, 2, \ldots, N_1. \tag{4b}$$

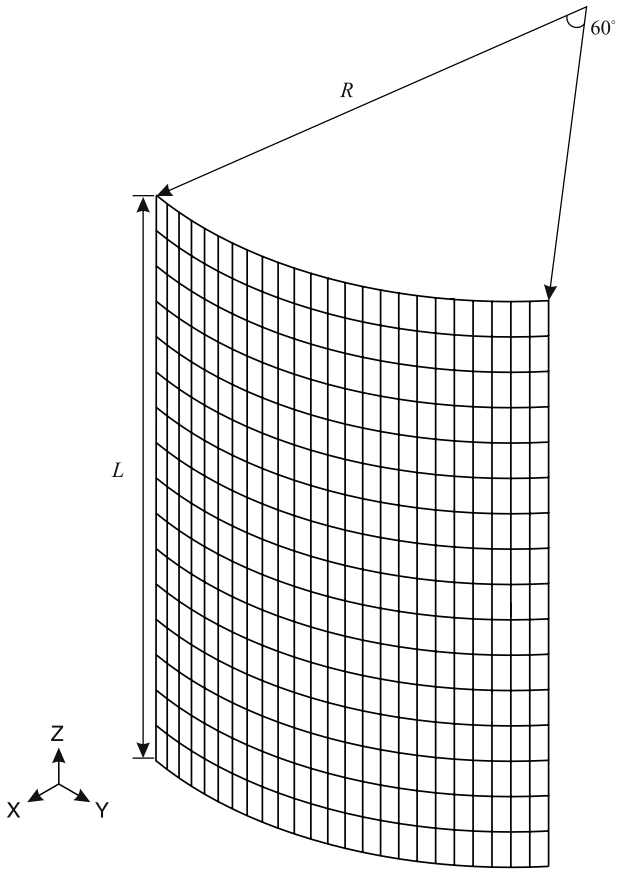

Fig. 4. Cylindrical panel problem ($L = 0.8$ m, $R = 0.5$ m, $h = 0.005$ m, $E = 69$ GPa, $\upsilon = 0.35$ and $\rho_s = 2700$ kg/m^3).

Note that the approximated original eigenvector $(\bar{\boldsymbol{\varphi}})_i$ can be obtained with $(\boldsymbol{\varphi}_1)_i$. While the formulation details differ among various DOFs based reduction methods, the general framework is similar.

2.2. Original formulation of Guyan reduction

Guyan reduction was developed using a reduction technique of the stiffness matrix in static analysis [27]. The linear static equations of the original structural model are

$$\mathbf{K}\mathbf{u} = \mathbf{f}, \tag{5}$$

in which, considering the master and slave DOFs, the stiffness matrix and displacement and force vectors are decomposed as

$$\mathbf{K} = \begin{bmatrix} \mathbf{K}_{11} & \mathbf{K}_{12} \\ \mathbf{K}_{21} & \mathbf{K}_{22} \end{bmatrix}, \qquad \mathbf{u} = \begin{bmatrix} \mathbf{u}_1 \\ \mathbf{u}_2 \end{bmatrix}, \qquad \mathbf{f} = \begin{bmatrix} \mathbf{f}_1 \\ \mathbf{f}_2 \end{bmatrix}. \tag{6}$$

Assuming that the slave force vector $\mathbf{f}_2$ is zero in Eq. (6), the slave displacement vector $\mathbf{u}_2$ can be represented by the master displacement vector $\mathbf{u}_1$

$$\mathbf{u}_2 = -\mathbf{K}_{22}^{-1}\mathbf{K}_{21}\mathbf{u}_1, \tag{7}$$

and, using Eqs. (6) and (7) in Eq. (5), the reduced stiffness matrix is obtained

$$\mathbf{K}_1 = \mathbf{K}_{11} - \mathbf{K}_{12}\mathbf{K}_{22}^{-1}\mathbf{K}_{21}. \tag{8}$$

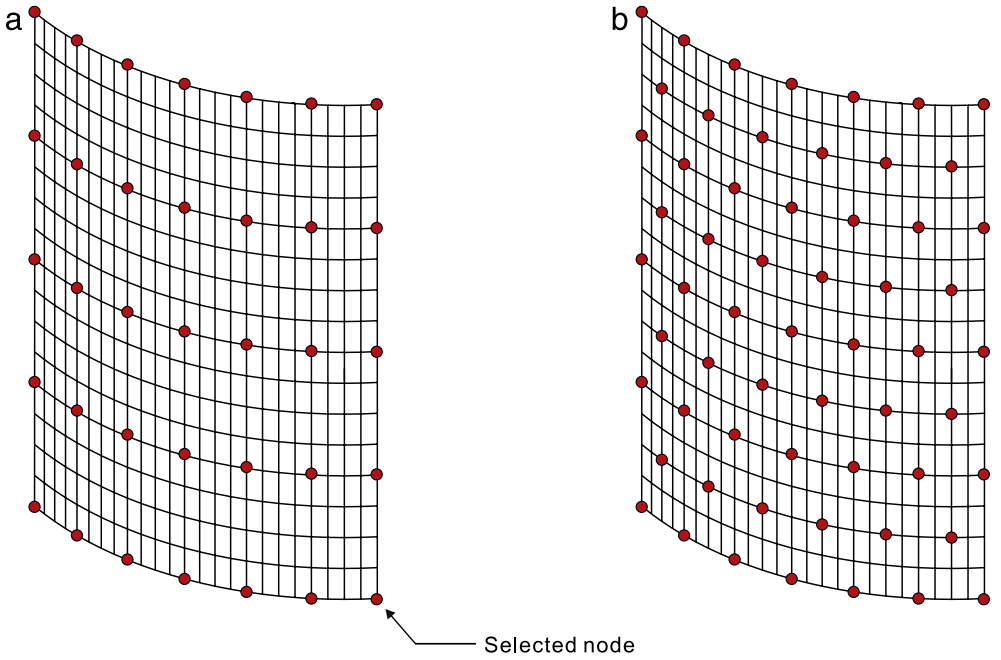

Fig. 5. Selected nodes in the cylindrical panel problem. (a) 35 nodes and (b) 59 nodes. At each selected node, all DOFs are considered as master DOFs.

Then, the original displacement vector $\mathbf{u}$ is approximated by the master displacement vector $\mathbf{u}_1$

$$\mathbf{u} \approx \bar{\mathbf{u}} = \mathbf{T}_G \mathbf{u}_1, \quad \mathbf{T}_G = \begin{bmatrix} \mathbf{I} \\ -\mathbf{K}_{22}^{-1}\mathbf{K}_{21} \end{bmatrix}, \tag{9}$$

where $\mathbf{T}_G$ is the original transformation matrix of Guyan reduction and $\mathbf{I}$ is an identity matrix.

Using $\mathbf{T}_G$ in Eq. (9), the reduced matrices are defined by

$$\mathbf{M}_1 = \mathbf{T}_G^T \mathbf{M} \mathbf{T}_G, \qquad \mathbf{K}_1 = \mathbf{T}_G^T \mathbf{K} \mathbf{T}_G. \tag{10}$$

Using Eq. (6) in Eq. (10), we can obtain the same reduced stiffness matrix $\mathbf{K}_1$ defined in Eq. (8). Similarly, $\mathbf{M}$ is also partitioned

$$\mathbf{M} = \begin{bmatrix} \mathbf{M}_{11} & \mathbf{M}_{12} \\ \mathbf{M}_{21} & \mathbf{M}_{22} \end{bmatrix}, \tag{11}$$

and the reduced mass matrix $\mathbf{M}_1$ is obtained as

$$\mathbf{M}_1 = \mathbf{M}_{11} - \mathbf{K}_{12}\mathbf{K}_{22}^{-1}\mathbf{M}_{21} - \mathbf{M}_{12}\mathbf{K}_{22}^{-1}\mathbf{K}_{21} + \mathbf{K}_{12}\mathbf{K}_{22}^{-1}\mathbf{M}_{22}\mathbf{K}_{22}^{-1}\mathbf{K}_{21}. \tag{12}$$

The reduced mass and stiffness matrices are used in the reduced eigenvalue problem in Eq. (3a). Using the ith calculated eigenvector $(\boldsymbol{\varphi}_1)_i$ and the transformation matrix $\mathbf{T}_G$, the original eigenvector $(\boldsymbol{\varphi})_i$ is approximated

$$(\boldsymbol{\varphi})_i \approx (\bar{\boldsymbol{\varphi}})_i = \mathbf{T}_G (\boldsymbol{\varphi}_1)_i. \tag{13}$$

2.3. Kidder's transformation matrix

In the original Guyan reduction process, the transformation matrix $\mathbf{T}_G$ is obtained considering only the stiffness matrix. To reduce errors due to the static condensation procedure in the original Guyan reduction, Kidder proposed a different derivation procedure for Guyan reduction [4].

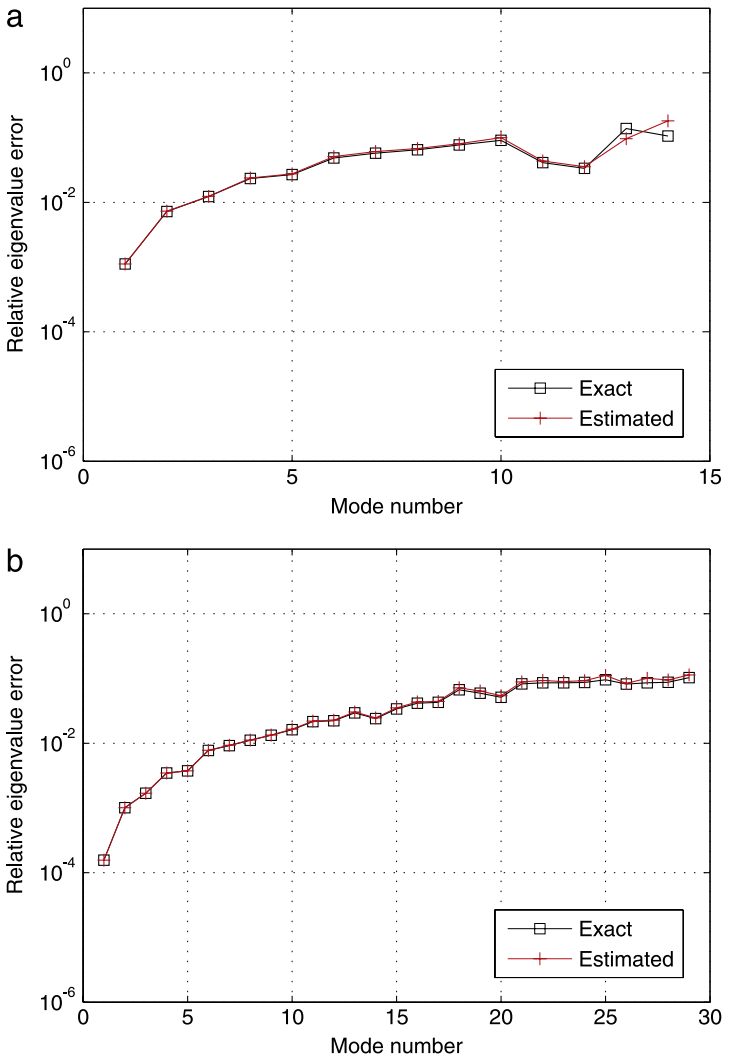

Fig. 6. Exact and estimated relative eigenvalue errors in the cylindrical panel problem. (a) 35 nodes and (b) 59 nodes.

Using the partitioned matrices in Eqs. (6) and (11), the original eigenvalue problem can be written as

$$\begin{bmatrix} \mathbf{K}_{11} & \mathbf{K}_{12} \\ \mathbf{K}_{21} & \mathbf{K}_{22} \end{bmatrix} \begin{bmatrix} \mathbf{u}_1 \\ \mathbf{u}_2 \end{bmatrix} = \lambda \begin{bmatrix} \mathbf{M}_{11} & \mathbf{M}_{12} \\ \mathbf{M}_{21} & \mathbf{M}_{22} \end{bmatrix} \begin{bmatrix} \mathbf{u}_1 \\ \mathbf{u}_2 \end{bmatrix}. \tag{14}$$

Using the second row in Eq. (14), the slave displacement vector $\mathbf{u}_2$ is defined by

$$\mathbf{u}_2 = [\mathbf{K}_{22} - \lambda \mathbf{M}_{22}]^{-1} [\lambda \mathbf{M}_{21} - \mathbf{K}_{21}] \mathbf{u}_1. \tag{15}$$

Note that Eq. (15) is the exact form of $\mathbf{u}_2$, see Eq. (7) for comparison.
Using Eq. (15) in the first row of Eq. (14), we obtain

$$\left\{ \mathbf{K}_{11} - \lambda \mathbf{M}_{11} - [\mathbf{K}_{12} - \lambda \mathbf{M}_{12}] [\mathbf{K}_{22} - \lambda \mathbf{M}_{22}]^{-1} [\mathbf{K}_{21} - \lambda \mathbf{M}_{21}] \right\} \mathbf{u}_1 = \mathbf{0}, \tag{16}$$

which is the exactly reduced eigenvalue problem. However, because λ is unknown, Eq. (16) can be solved using an iterative solution technique, and the inverse of $[\mathbf{K}_{22} - \lambda \mathbf{M}_{22}]$ needs to be calculated during each iteration step. To

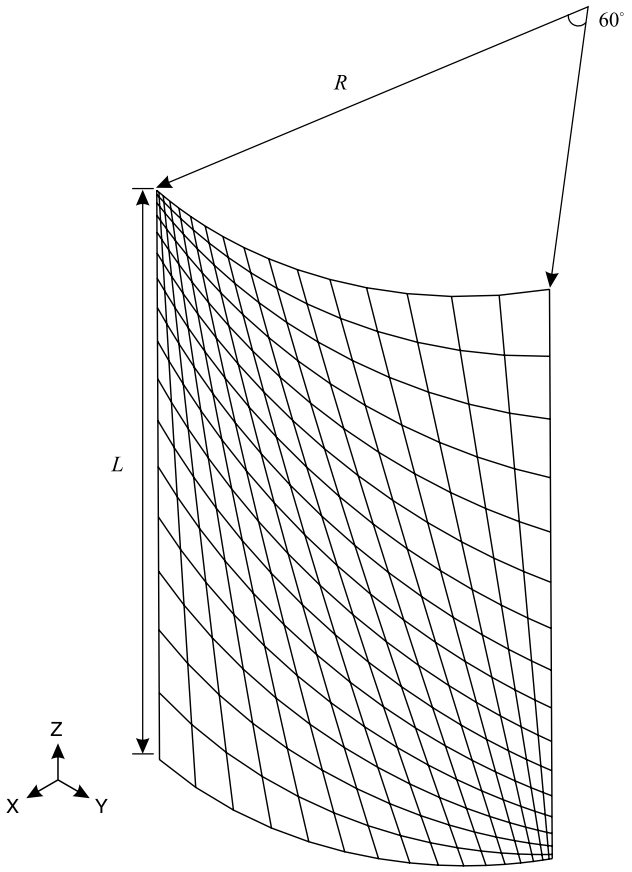

Fig. 7. Cylindrical panel problem with a distorted mesh ($L = 0.8$ m, $R = 0.5$ m, $h = 0.005$ m, $E = 69$ GPa, $\upsilon = 0.35$ and $\rho_s = 2700$ kg/m^3).

reduce the computational cost, the inverse term can be expanded as

$$[\mathbf{K}_{22} - \lambda \mathbf{M}_{22}]^{-1} = \mathbf{K}_{22}^{-1} + \lambda \mathbf{K}_{22}^{-1}\mathbf{M}_{22}\mathbf{K}_{22}^{-1} + O\left(\lambda^2\right) + O\left(\lambda^3\right) + \cdots. \tag{17}$$

Substituting Eq. (17) into Eq. (16) and neglecting the higher order terms of λ (more than 2nd order), the following reduced equations are obtained

$$[\mathbf{K}_1 - \lambda \mathbf{M}_1]\,\mathbf{u}_1 = \mathbf{0}, \tag{18}$$

and also

$$\mathbf{u}_2 = [\mathbf{K}_{22}^{-1} + \lambda \mathbf{K}_{22}^{-1}\mathbf{M}_{22}\mathbf{K}_{22}^{-1}][\lambda\, \mathbf{M}_{21} - \mathbf{K}_{21}]\mathbf{u}_1, \tag{19}$$

in which the obtained reduced matrices $\mathbf{M}_1$ and $\mathbf{K}_1$ are identical to those in the original Guyan reduction process, see Eqs. (8) and (12). That is, the final reduced eigenvalue problem by Kidder's approach is identical to that of the original Guyan reduction process.

However, the slave displacement vector $\mathbf{u}_2$ in Eq. (19) is more accurately calculated than the original one in Eq. (7). The original displacement vector $\mathbf{u}$ is then approximated by

$$\mathbf{u} \approx \bar{\mathbf{u}} = \mathbf{T}_K \mathbf{u}_1, \quad \mathbf{T}_K = \begin{bmatrix} \mathbf{I} \\ \left[\mathbf{K}_{22}^{-1} + \lambda \mathbf{K}_{22}^{-1}\mathbf{M}_{22}\mathbf{K}_{22}^{-1}\right][\lambda \mathbf{M}_{21} - \mathbf{K}_{21}] \end{bmatrix}, \tag{20}$$

where $\mathbf{T}_K$ is Kidder's transformation matrix, which is an enhanced form of the original transformation matrix $\mathbf{T}_G$. The transformation matrix $\mathbf{T}_K$ can be expressed by the sum of the original transformation matrix $\mathbf{T}_G$ and the residual

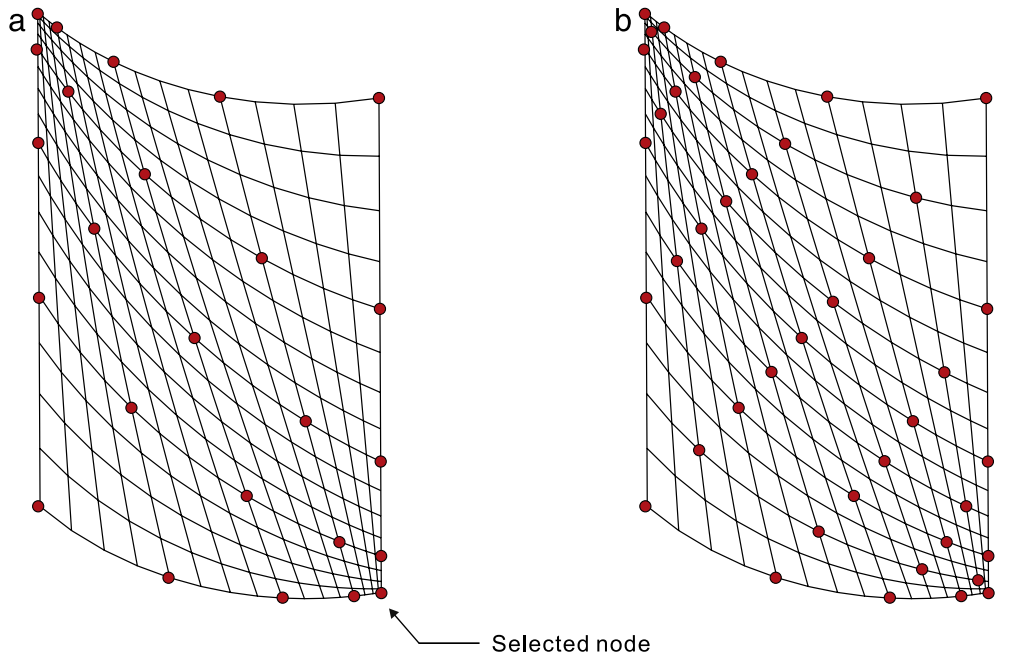

Fig. 8. Selected nodes in the cylindrical panel problem with a distorted mesh. (a) 25 nodes and (b) 41 nodes. At each selected node, all DOFs are considered as master DOFs.

matrix denoted by $\mathbf{T}_r$

$$\mathbf{T}_K = \mathbf{T}_G + \mathbf{T}_r, \quad \mathbf{T}_r = \begin{bmatrix} \mathbf{0} \\ \lambda\left[\mathbf{K}_{22}^{-1}\mathbf{M}_{21} - \mathbf{K}_{22}^{-1}\mathbf{M}_{22}\mathbf{K}_{22}^{-1}\mathbf{K}_{21}\right] + \lambda^2\mathbf{K}_{22}^{-1}\mathbf{M}_{22}\mathbf{K}_{22}^{-1}\mathbf{M}_{21} \end{bmatrix}. \tag{21}$$

Note that, unlike the transformation matrix $\mathbf{T}_G$ in the original Guyan reduction, the term of λ^2 is contained in Kidder's transformation matrix $\mathbf{T}_K$. For this reason, using Kidder's transformation matrix $\mathbf{T}_K$, the ith original eigenvector $(\boldsymbol{\varphi})_i$ is more accurately approximated by

$$(\boldsymbol{\varphi})_i \approx (\bar{\boldsymbol{\varphi}})_i = \mathbf{T}_K(\boldsymbol{\varphi}_1)_i = (\mathbf{T}_G + \mathbf{T}_r)a(\boldsymbol{\varphi}_1)_i. \tag{22}$$

It is important to note that the two approaches produce the same reduced matrices $\mathbf{M}_1$ and $\mathbf{K}_1$, and thus the same eigensolutions $(\bar{\lambda}_i, (\boldsymbol{\varphi}_1)_i)$ are obtained from Eq. (3a).

3. Derivation of the error estimator

To evaluate the accuracy of the approximated eigensolutions for the reduced eigenvalue problem, the following relative eigenvalue error is generally used

$$\xi_i = \frac{\bar{\lambda}_i}{\lambda_i} - 1, \tag{23}$$

in which ξ_i denotes the ith relative eigenvalue error and λ_i is the ith exact eigenvalue of the original model obtained from the original eigenvalue problem in Eq. (1).

In this section, we introduce a method to estimate the relative eigenvalue error in Eq. (23) without knowing the exact eigenvalue λ_i. The similar derivation procedure has been recently employed for the Craig–Bampton method [28].

Since λ_i and $(\boldsymbol{\varphi})_i$ are the eigensolutions of the original eigenvalue problem in Eq. (1), the following equation should be satisfied

$$\frac{1}{\lambda_i}(\boldsymbol{\varphi})_i^T\mathbf{K}(\boldsymbol{\varphi})_i = (\boldsymbol{\varphi})_i^T\mathbf{M}(\boldsymbol{\varphi})_i. \tag{24}$$

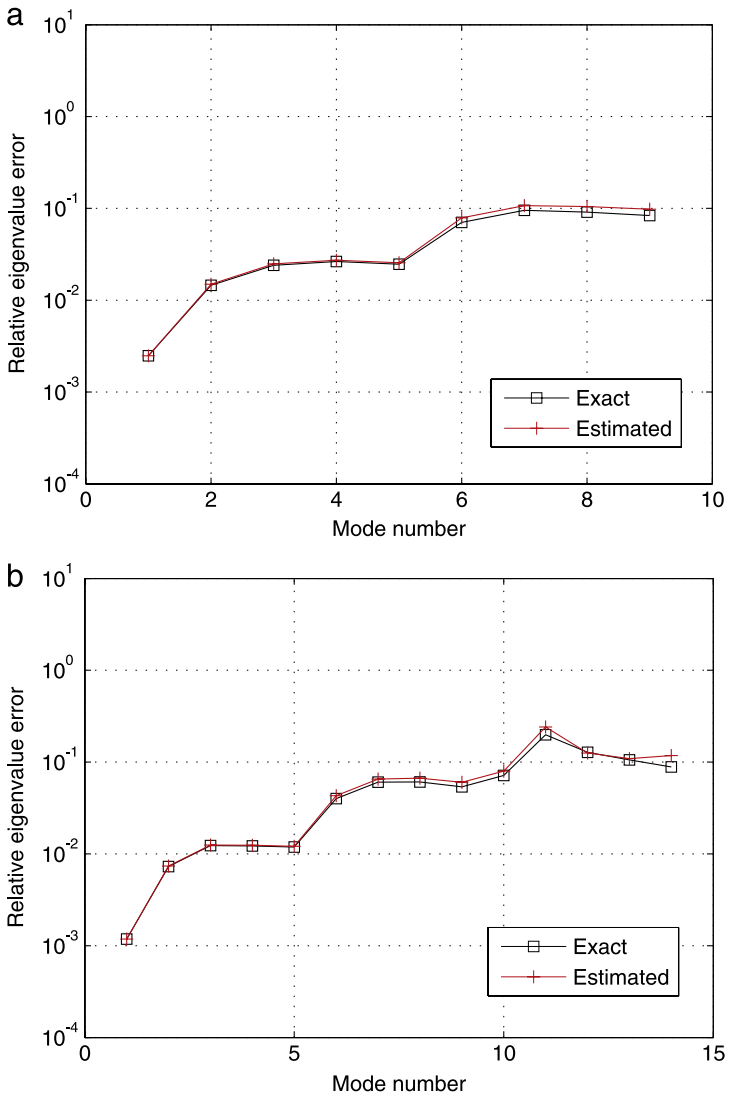

Fig. 9. Exact and estimated relative eigenvalue errors in the cylindrical panel problem with a distorted mesh. (a) 25 nodes and (b) 41 nodes.

The original eigenvector $(\boldsymbol{\varphi})_i$ can be expressed as the approximated and error parts as

$$(\boldsymbol{\varphi})_i = (\bar{\boldsymbol{\varphi}})_i + (\delta\boldsymbol{\varphi})_i, \tag{25}$$

in which $(\delta\boldsymbol{\varphi})_i$ is an error in the approximated eigenvector.

Substituting Eq. (25) into Eq. (24), we obtain four scalar terms

$$\frac{1}{\lambda_i}(\bar{\boldsymbol{\varphi}})_i^T \mathbf{K}(\bar{\boldsymbol{\varphi}})_i - (\bar{\boldsymbol{\varphi}})_i^T \mathbf{M}(\bar{\boldsymbol{\varphi}})_i - \frac{1}{\lambda_i}(\delta\boldsymbol{\varphi})_i^T \mathbf{K}(\delta\boldsymbol{\varphi})_i + (\delta\boldsymbol{\varphi})_i^T \mathbf{M}(\delta\boldsymbol{\varphi})_i = 0. \tag{26}$$

Using Eq. (22) in Eq. (26), we obtain

$$\frac{1}{\lambda_i}(\boldsymbol{\varphi}_1)_i^T \left[\mathbf{T}_G + \mathbf{T}_r\right]^T \mathbf{K} \left[\mathbf{T}_G + \mathbf{T}_r\right](\boldsymbol{\varphi}_1)_i - (\boldsymbol{\varphi}_1)_i^T \left[\mathbf{T}_G + \mathbf{T}_r\right]^T \mathbf{M} \left[\mathbf{T}_G + \mathbf{T}_r\right](\boldsymbol{\varphi}_1)_i$$
$$- \frac{1}{\lambda_i}(\delta\boldsymbol{\varphi})_i^T \left[\mathbf{K} - \lambda_i \mathbf{M}\right](\delta\boldsymbol{\varphi})_i = 0. \tag{27}$$

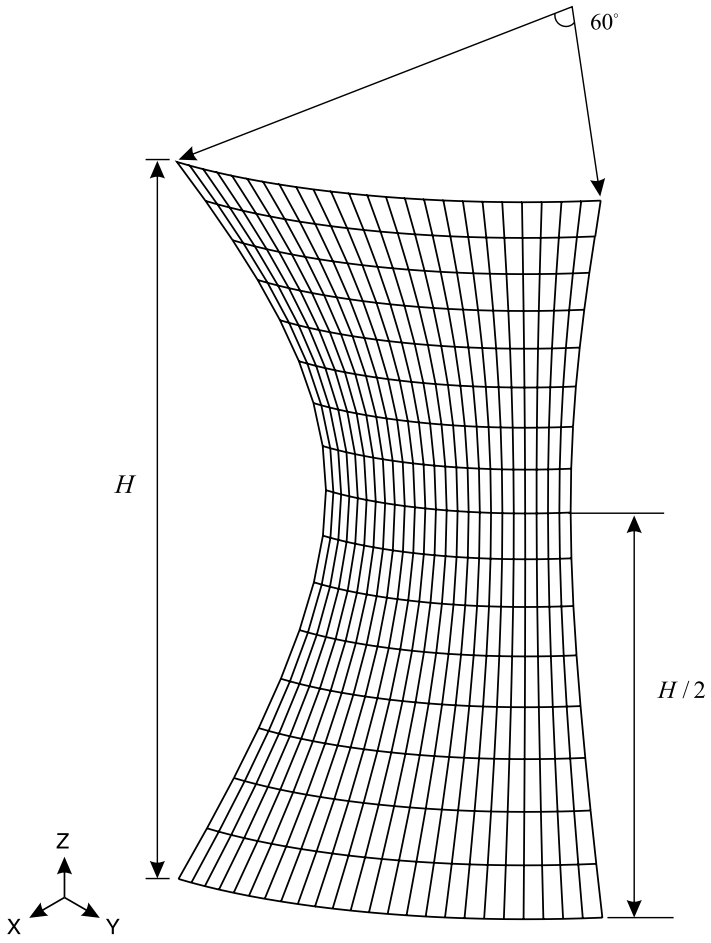

Fig. 10. Hyperboloid panel problem ($H = 4$ m, $h = 0.005$m, $E = 69$ GPa, $\upsilon = 0.35$ and $\rho_s = 2700\,\mathrm{kg/m^3}$).

After expanding Eq. (27) and applying the mass-orthonormality and stiffness-orthogonality conditions for the reduced eigenvalue problem in Eq. (4), the following equation is obtained

$$\frac{\bar{\lambda}_i}{\lambda_i} - 1 = 2(\boldsymbol{\varphi}_1)_i^T \mathbf{T}_G^T \left[\mathbf{M} - \frac{1}{\lambda_i}\mathbf{K}\right] \mathbf{T}_r (\boldsymbol{\varphi}_1)_i + (\boldsymbol{\varphi}_1)_i^T \mathbf{T}_r^T \left[\mathbf{M} - \frac{1}{\lambda_i}\mathbf{K}\right] \mathbf{T}_r (\boldsymbol{\varphi}_1)_i + \frac{1}{\lambda_i} (\delta\boldsymbol{\varphi})_i^T \left[\mathbf{K} - \lambda_i \mathbf{M}\right] (\delta\boldsymbol{\varphi})_i, \tag{28}$$

in which the left-hand side is the relative eigenvalue error in Eq. (23).

When the approximated original eigenvectors $(\bar{\boldsymbol{\varphi}})_i$ are close enough to the exact original eigenvectors $(\boldsymbol{\varphi})_i$ (that is, $(\boldsymbol{\varphi})_i \approx (\bar{\boldsymbol{\varphi}})_i$), it is possible to assume that

$$\frac{1}{\lambda_i}(\bar{\boldsymbol{\varphi}})_i^T \mathbf{K} (\bar{\boldsymbol{\varphi}})_i \approx 1 \quad \text{and} \quad \frac{1}{\lambda_i}(\bar{\boldsymbol{\varphi}})_i^T \mathbf{K} (\bar{\boldsymbol{\varphi}})_i \gg \frac{1}{\lambda_i}(\delta\boldsymbol{\varphi})_i^T \mathbf{K} (\delta\boldsymbol{\varphi})_i, \tag{29a}$$

$$(\bar{\boldsymbol{\varphi}})_i^T \mathbf{M} (\bar{\boldsymbol{\varphi}})_i \approx 1 \quad \text{and} \quad (\bar{\boldsymbol{\varphi}})_i^T \mathbf{M} (\bar{\boldsymbol{\varphi}})_i \gg (\delta\boldsymbol{\varphi})_i^T \mathbf{M} (\delta\boldsymbol{\varphi})_i. \tag{29b}$$

Under the assumption in Eq. (29a), we neglect the last term on the right-hand side of Eq. (28)

$$\frac{\bar{\lambda}_i}{\lambda_i} - 1 \approx 2(\boldsymbol{\varphi}_1)_i^T \mathbf{T}_G^T \left[\mathbf{M} - \frac{1}{\lambda_i}\mathbf{K}\right] \mathbf{T}_r (\boldsymbol{\varphi}_1)_i + (\boldsymbol{\varphi}_1)_i^T \mathbf{T}_r^T \left[\mathbf{M} - \frac{1}{\lambda_i}\mathbf{K}\right] \mathbf{T}_r (\boldsymbol{\varphi}_1)_i. \tag{30}$$

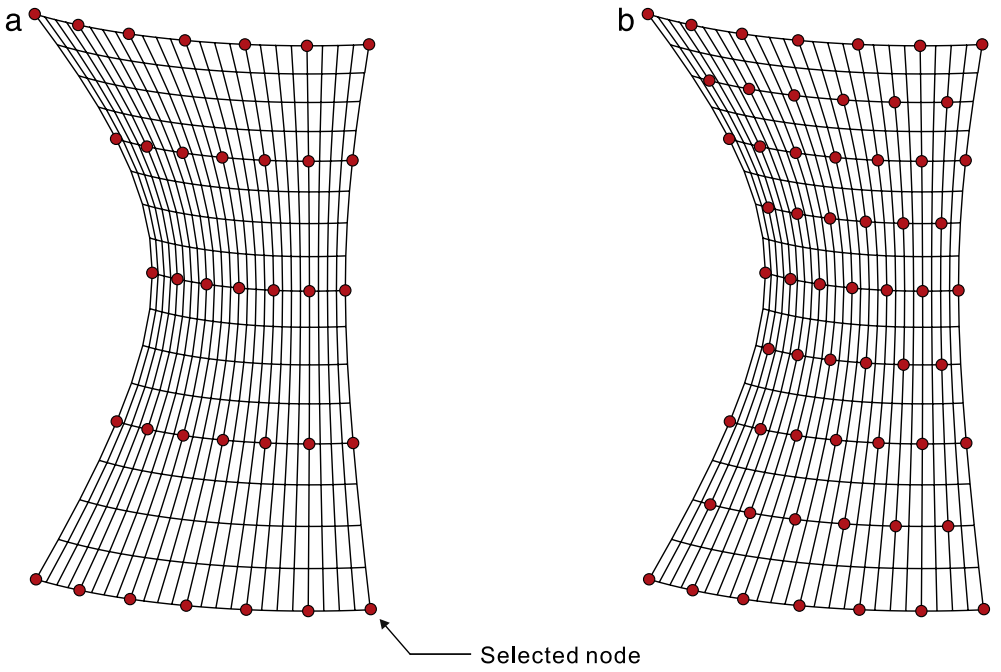

Fig. 11. Selected nodes in the hyperboloid panel problem. (a) 35 nodes and (b) 59 nodes. At each selected node, all DOFs are considered as master DOFs.

Finally, we propose an error estimator η_i for the ith relative eigenvalue error

$$\eta_i = 2(\boldsymbol{\varphi}_1)_i^T \mathbf{T}_G^T \left[\mathbf{M} - \frac{1}{\bar{\lambda}_i}\mathbf{K}\right] \mathbf{T}_r (\boldsymbol{\varphi}_1)_i + (\boldsymbol{\varphi}_1)_i^T \mathbf{T}_r^T \left[\mathbf{M} - \frac{1}{\bar{\lambda}_i}\mathbf{K}\right] \mathbf{T}_r (\boldsymbol{\varphi}_1)_i, \tag{31}$$

with

$$\mathbf{T}_r = \begin{bmatrix} \mathbf{0} \\ \bar{\lambda}_i \left[\mathbf{K}_{22}^{-1}\mathbf{M}_{21} - \mathbf{K}_{22}^{-1}\mathbf{M}_{22}\mathbf{K}_{22}^{-1}\mathbf{K}_{21}\right] + \bar{\lambda}_i^2 \mathbf{K}_{22}^{-1}\mathbf{M}_{22}\mathbf{K}_{22}^{-1}\mathbf{M}_{21} \end{bmatrix}, \tag{32}$$

in which, to approximate λ_i contained in Eq. (21), we use the ith approximated eigenvalue $\bar{\lambda}_i$ calculated from the reduced eigenvalue problem instead of λ_i.

In general, reduced models more accurately approximate lower modes than higher modes. Therefore, the assumption in Eq. (29) would not be well applied to the estimation of relative eigenvalue errors corresponding to higher modes. For this reason, the proposed error estimator η_i will give a more accurate estimation for relative eigenvalue errors corresponding to lower modes.

It should be also noted that the sign of the last term on the right-hand side of Eq. (28) varies depending on the mode number. For this reason, it is not easy to theoretically identify whether the proposed error estimator η_i is an upper or lower bound for a specific relative eigenvalue error ξ_i. This issue will be discussed in more detail in the following section.

In Eqs. (31) and (32), we can easily identify the fact that the computational cost of the error estimator η_i is low. In those equations, we reuse the matrix $\mathbf{K}_{22}^{-1}$ previously calculated in Eq. (9), and the required matrix operations are merely simple additions and multiplications.

4. Numerical examples

In this section, we present the performance of the proposed error estimator η_i. Four structural problems are considered: rectangular plate, cylindrical panel, hyperboloid panel, and shaft–shaft interaction problems. For the finite element modeling, we use the well-known 4-node MITC shell finite elements, in which shear locking is effectively alleviated [29–33].

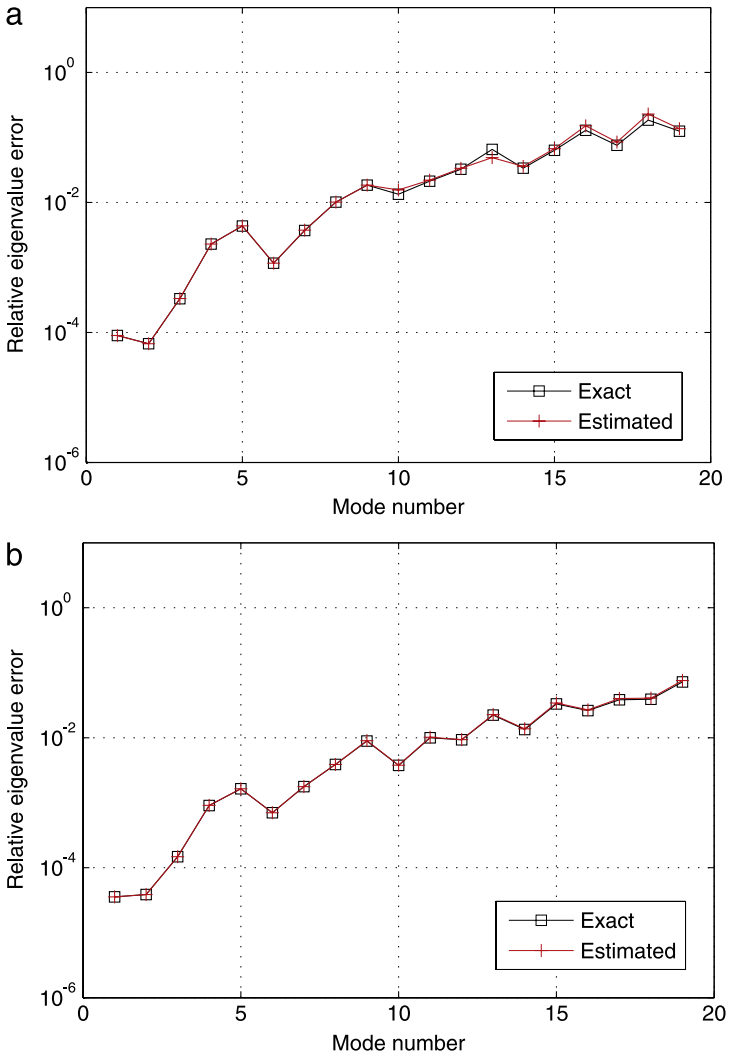

Fig. 12. Exact and estimated relative eigenvalue errors in the hyperboloid panel problem. (a) 35 nodes and (b) 59 nodes.

As mentioned in Introduction, there is no previous error estimator that can provide relative eigenvalue errors. Therefore, we simply show the performance of the proposed error estimator without comparisons in the following sections.

4.1. Rectangular plate problem

Let us consider a rectangular plate with free boundary, see Fig. 1. Length L is 3 m, width B is 2 m, and thickness h is 0.008 m. Young's modulus E is 69 GPa, Poisson's ratio ν is 0.35, and density ρ_s is 2700 kg/m^3. In the model, we use a uniform 12×8 mesh of shell finite elements, in which 117 nodes, 96 elements and 351 DOFs are contained. We consider two numerical cases with different master DOFs selected. The master DOFs are selected as shown in Fig. 2(a) and (b).

We first calculate the exact and estimated relative eigenvalue errors from the lowest eigenvalue. As shown in Fig. 3, the results show the excellent performance of the proposed error estimator. The exact and estimated relative eigenvalue errors are specifically listed in Table 1. As expected in the previous section, more accurate error estimation results are obtained for the relative eigenvalue errors corresponding to lower modes, and the present error estimator η_i acts like an upper bound of the relative eigenvalue error ξ_i in the numerical cases considered.

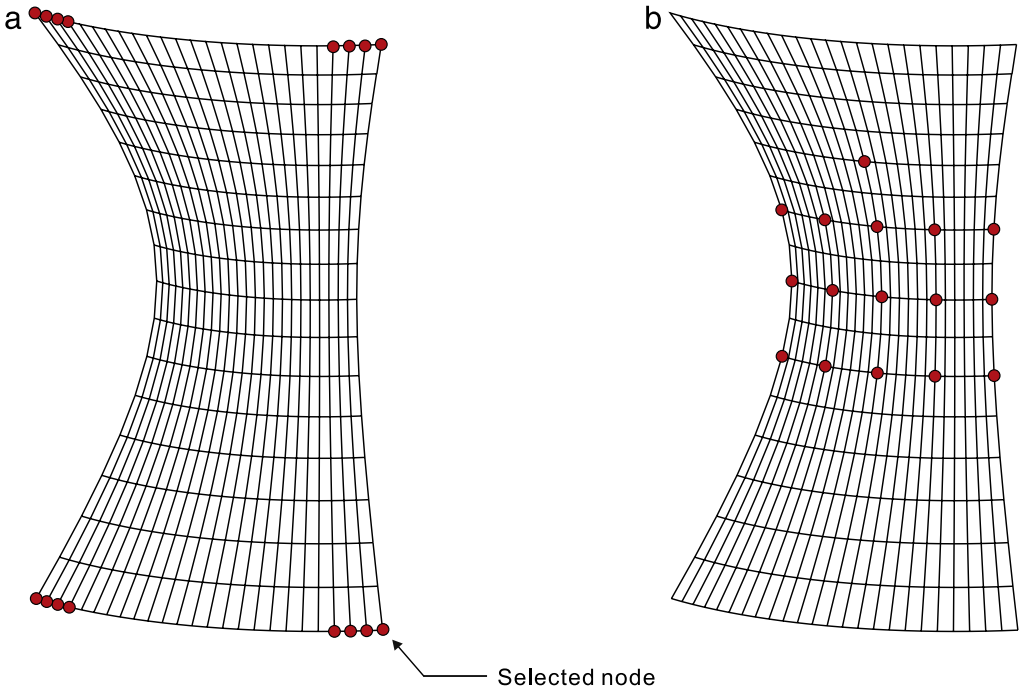

Fig. 13. Selected nodes in the hyperboloid panel problem. (a) 16 nodes selected by the DOFs selection criterion [21,22] and (b) 16 nodes selected badly. At each selected node, all DOFs are considered as master DOFs.

We additionally calculate the approximated eigenvalues and their relative errors when the shift and invert spectral transformation (SI) is used in the reduced model [34]. The shifts are performed from the 4th and 10th modes in the cases in Fig. 2(a) and (b), respectively. The error estimation performance is still good, see Fig. 3.

4.2. Cylindrical panel problem

We here apply the proposed error estimator to a cylindrical panel with free boundary, see Fig. 4. Length L is 0.8 m, radius R is 0.5 m, and thickness h is 0.005 m. Young's modulus E is 69 GPa, Poisson's ratio ν is 0.35, and density ρ_s is 2700 kg/m^3. The cylindrical panel is modeled by a 24×16 uniform mesh of shell finite elements (2125 DOFs).

Two cases of master DOFs selection are considered as shown in Fig. 5. Fig. 6 shows that the proposed error estimator very accurately estimates the exact relative eigenvalue errors. The exact and estimated relative eigenvalue errors are listed in Table 2. It is observed that the error estimator η_i generally acts likes an upper bound for the relative eigenvalue error ξ_i except for the 13th mode in the case of 35 nodes selected.

The performance of the proposed error estimator is also tested in a distorted mesh case, see Fig. 7. The cylindrical panel is modeled by a 16×16 distorted mesh of shell finite elements [33]. Two numerical cases with differently selected master DOFs are considered as shown in Fig. 8(a) and (b). Fig. 9 shows that the present error estimator performs well in the distorted mesh.

4.3. Hyperboloid panel problem

We consider a hyperboloid panel of height $H = 4$ m and thickness $h = 0.005$ m. The mid-surface of the shell structure is described by

$$x^2 + y^2 = 2 + z^2; \quad z \in [-2, 2]\,. \tag{33}$$

No boundary condition is imposed. Young's modulus E is 69 GPa, Poisson's ratio ν is 0.35, and density ρ_s is 2700 kg/m^3. A 24×16 mesh of shell finite elements is used, see Fig. 10.

Two numerical cases with differently selected master DOFs are considered as shown in Fig. 11(a) and (b). The excellent performance of the proposed error estimator is observed in Fig. 12 for the two numerical cases.

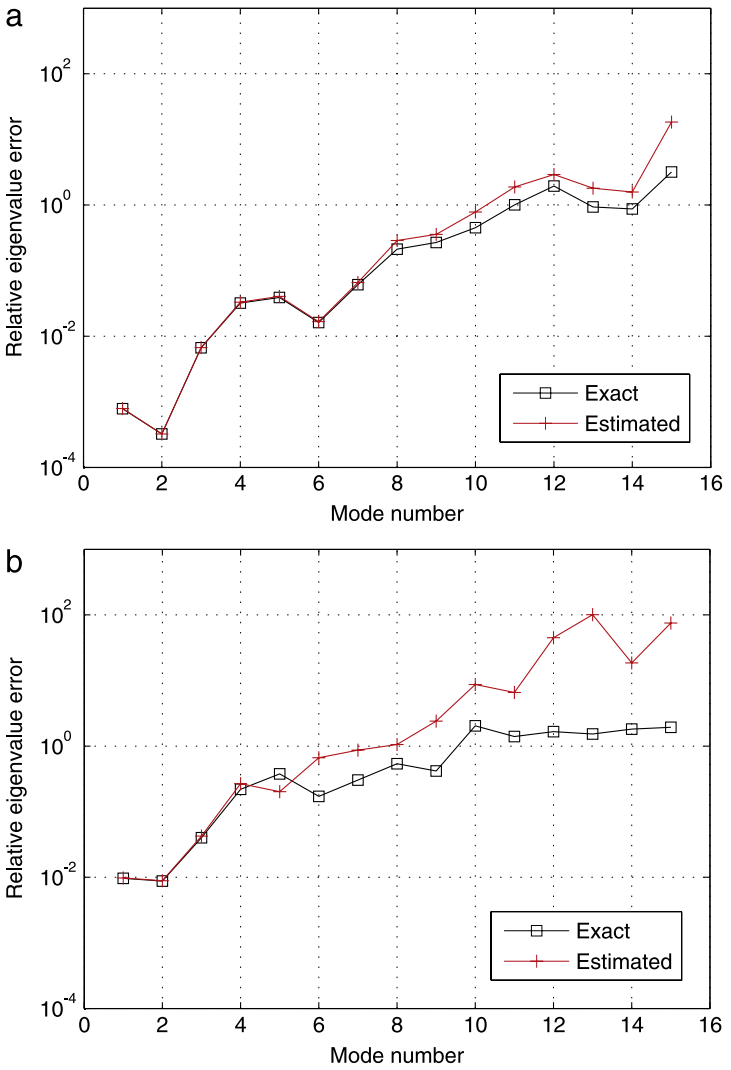

Fig. 14. Exact and estimated relative eigenvalue errors in the hyperboloid panel problem. (a) 16 nodes selected by the DOFs selection criterion [21,22] and (b) 16 nodes selected badly.

In Section 3, the assumption based on $(\boldsymbol{\varphi})_i \approx (\bar{\boldsymbol{\varphi}})_i$ in Eq. (31) is used to derive the proposed error estimator. Therefore, the performance of the error estimator depends on how well the master DOFs are selected. To investigate the effect of the master DOFs selection, only 16 master nodes are selected using two different ways:

- Case (a): A well-known DOFs selection criterion based on the ratio of the diagonal terms of mass and stiffness matrices (K_{ii}/M_{ii}) is employed [18,19], see Fig. 13(a).
- Case (b): To exemplify a badly selected case, the master nodes are selected as shown in Fig. 13(b). Therefore, in Case (b), the condition $(\boldsymbol{\varphi})_i \approx (\bar{\boldsymbol{\varphi}})_i$ is less satisfied than in Case (a).

Fig. 14 shows that the overall error estimation accuracy is better in Case (a) and, of course, the accuracy of eigensolution is also better in Case (a). Therefore, when the master DOFs are badly selected, the proposed error estimator should be carefully used.

4.4. Shaft–shaft interaction problem

We consider two cylindrical shafts connected with fillets with a radius 0.002 m and no boundary condition is imposed, see Fig. 15. Height H is 0.08 m and thickness h is 0.0005 m. The radii R_1 and R_2 are 0.01m and 0.0075 m,

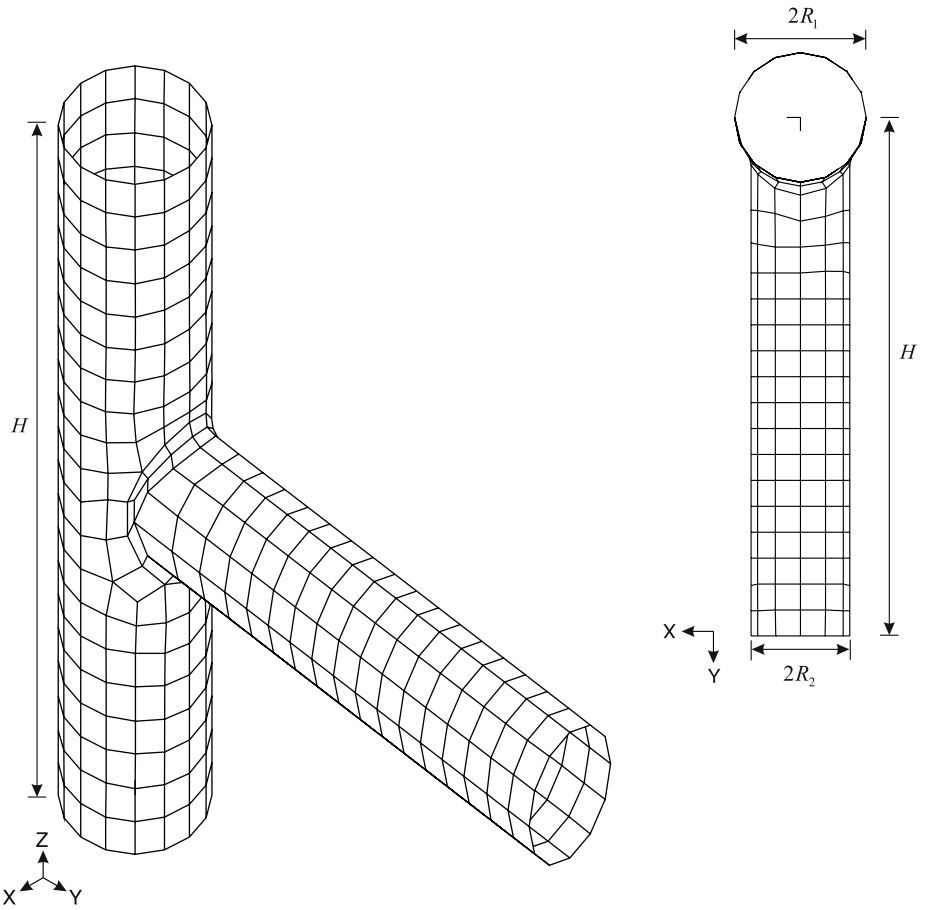

Fig. 15. Shaft–shaft interaction problem ($H = 0.08$ m, $h = 0.0005$ m, $R_1 = 0.01$ m, $R_2 = 0.0075$ m, $E = 207$ GPa, $\upsilon = 0.29$ and $\rho_s = 2700\,\mathrm{kg/m^3}$).

Table 2
Exact and estimated eigenvalue errors in the cylindrical panel problem.

Mode number	(a) Case of 35 nodes selected		(b) Case of 59 nodes selected	
	Exact	Estimated	Exact	Estimated
1	1.12350E−03	1.12483E−03	1.56297E−04	1.56322E−04
2	7.23810E−03	7.29471E−03	1.01049E−03	1.01154E−03
3	1.22849E−02	1.24491E−02	1.68794E−03	1.69086E−03
4	2.33257E−02	2.38409E−02	3.45928E−03	3.47110E−03
5	2.67692E−02	2.74654E−02	3.73763E−03	3.75156E−03
6	4.85401E−02	5.11211E−02	7.73819E−03	7.80110E−03
7	5.73569E−02	6.09591E−02	9.19521E−03	9.28327E−03
8	6.49595E−02	6.78828E−02	1.11228E−02	1.12428E−02
9	7.68949E−02	8.07779E−02	1.32702E−02	1.34415E−02
10	9.11205E−02	1.00272E−01	1.62110E−02	1.64882E−02
11	4.11632E−02	4.35197E−02	2.15578E−02	2.20170E−02
12	3.36082E−02	3.54133E−02	2.22282E−02	2.27205E−02
13	1.37641E−01	9.61562E−02	2.94087E−02	3.03196E−02
14	1.06411E−01	1.81928E−01	2.39770E−02	2.45508E−02

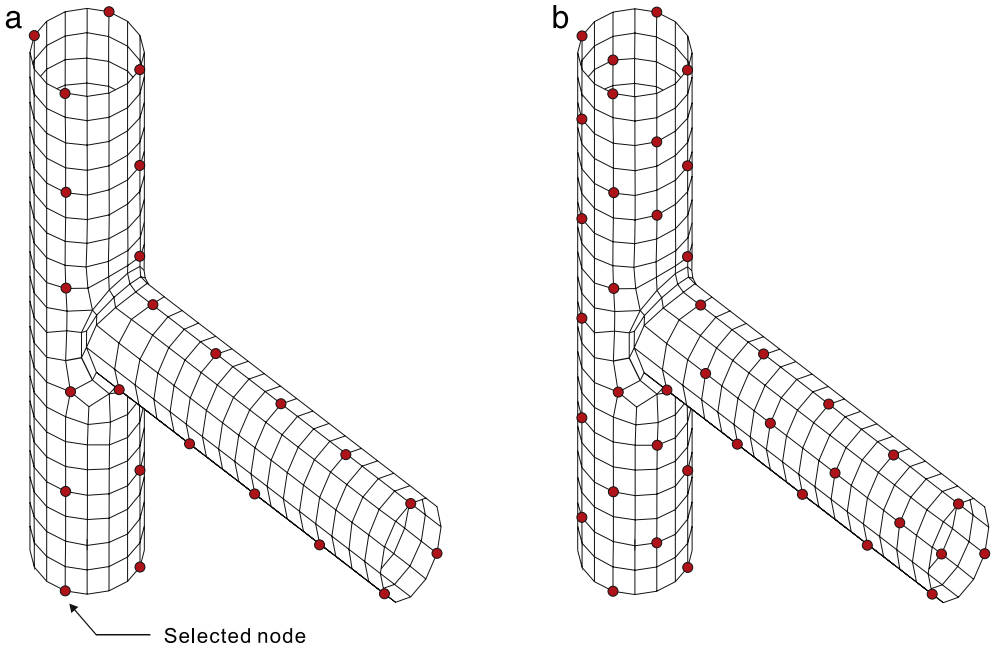

Fig. 16. Selected nodes of the shaft–shaft interaction problem. (a) 39 nodes and (b) 70 nodes. At each selected node, all DOFs are considered as master DOFs.

respectively. Young's modulus E is 207 GPa, Poisson's ratio ν is 0.29, and density ρ_s is 2700 kg/m^3. In this problem, 534 shell finite elements and 555 nodes are used.

We consider two differently selected master DOFs in Fig. 16. The exact and estimated eigenvalue errors are compared in Fig. 17. The proposed error estimator consistently shows the excellent performance.

In this paper, only undamped structural models are considered, but the proposed error estimator would be also employed for model reductions of damped structural models [35].

5. Conclusions

In this paper, we developed an accurate error estimator for Guyan reduction which can estimate relative eigenvalue errors in reduced models. Therefore, the error estimator can provide the reliability of models reduced by Guyan reduction. The proposed error estimator is derived from the original eigenvalue problem using Kidder's transformation matrix. The resulting error estimator is simple and computationally inexpensive. The excellent performance of the proposed error estimator was demonstrated through various numerical examples.

It is important to note that, using a similar derivation procedure, error estimators could be developed for other DOFs based reduction methods such as the improved reduced system (IRS) method. Then, such error estimators could be utilized together with DOFs selection methods [18–22] and iterative procedures (i.e., the iterative IRS method and the iterative order reduction (IOR) method [9,10,12]) to develop more effective DOFs based reduction methods.

Acknowledgments

This work was supported by the Human Resources Development program (No. 20134030200300) of the Korea Institute of Energy Technology Evaluation and Planning (KETEP) grant funded by the Korea government Ministry of Trade, Industry and Energy. This research was also supported by a grant [NEMA-ETH-2012-05] from the Earthquake and Tsunami Hazard Mitigation Research Group, National Emergency Management Agency of Korea.

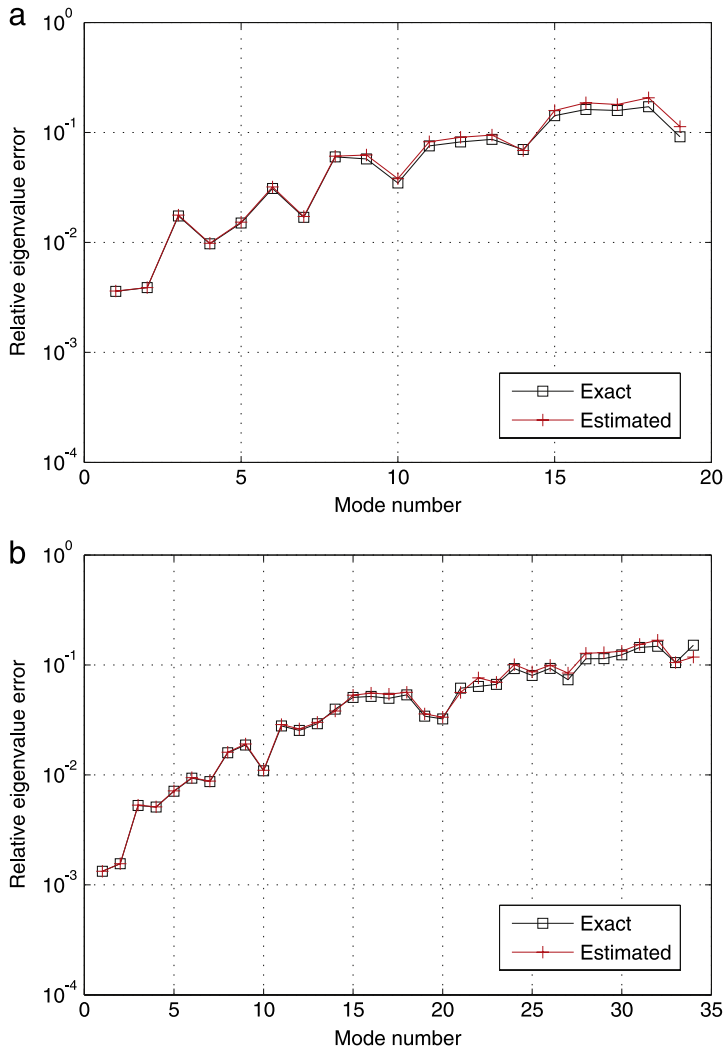

Fig. 17. Exact and estimated relative eigenvalue errors in the shaft–shaft interaction problem. (a) 39 nodes and (b) 70 nodes.

References

[1] R. Guyan, Reduction of stiffness and mass matrices, AIAA J. 3 (2) (1965) 380.
[2] B.M. Irons, Eigenvalue economisers in vibration problems, J. Roy. Aeronaut. Soc. 67 (1963) 526.
[3] B.M. Irons, Structural eigenvalue problems: elimination of unwanted variables, AIAA J. 3 (1965) 961.
[4] R.L. Kidder, Reduction of structural frequency equations, AIAA J. 11 (6) (1973) 892.
[5] E.J. Kuhar, C.V. Stahle, Dynamic transformation method for modal synthesis, AIAA J. 12 (5) (1974) 672–678.
[6] Y.T.L. Leung, An accurate method of dynamic condensation in structural analysis, Internat. J. Numer. Methods Engrg. 21 (1978) 1705–1715.
[7] J. O'Callanhan, A procedure for an improved reduced system (IRS) model, in: Proceeding the 7th International Modal Analysis Conference, Bethel, CT, 1989.
[8] L.E. Suarez, Dynamic condensation method for structural eigenvalue analysis, AIAA J. 30 (4) (1992) 1046–1054.
[9] M.I. Friswell, S.D. Garvey, J.E.T. Penny, Model reduction using dynamic and iterated IRS techniques, J. Sound Vib. 186 (2) (1995) 311–323.
[10] M.I. Friswell, S.D. Garvey, J.E.T. Penny, The convergence of the iterated IRS method, J. Sound Vib. 211 (1) (1998) 123–132.
[11] K.O. Kim, M.K. Kang, Convergence acceleration of iterative modal reduction methods, AIAA J. 39 (1) (2001) 134–140.
[12] Y. Xia, R. Lin, A new iterative order reduction (IOR) method for eigensolutions of large structures, Internat. J. Numer. Methods Engrg. 59 (2004) 153–172.
[13] D. Choi, H. Kim, M. Cho, Iterative method for dynamic condensation combined with substructuring scheme, J. Sound Vib. 317 (1–2) (2008) 199–218.
[14] M.P. Singh, L.E. Suarez, Dynamic condensation with synthesis of substructure eigenproperties, J. Sound Vib. 159 (1) (1992) 139–155.

[15] N. Bouhaddi, R. Fillod, A method for selecting master DOF in dynamic substructuring using the Guyan condensation method, Comput. Struct. 45 (5) (1992) 941–946.
[16] N. Bouhaddi, R. Fillod, Substructuring by a two level dynamic condensation method, Comput. Struct. 60 (3) (1996) 403–409.
[17] H. Kim, M. Cho, Improvement of reduction method combined with sub-domain scheme in large-scale problem, Internat. J. Numer. Methods Engrg. 70 (2007) 206–251.
[18] R.D. Henshell, J.H. Ong, Automatic masters from eigenvalues economization, Earthq. Eng. Struct. Dyn. 3 (1975) 375–383.
[19] J.H. Ong, Improved automatic masters for eigenvalues economization, Finite Elem. Anal. Des. 3 (2) (1987) 149–160.
[20] V.N. Shah, M. Raymund, Analytical selection of masters for the reduced eigenvalue problem, Internat. J. Numer. Methods Engrg. 18 (1) (1982) 89–98.
[21] K.O. Kim, Y.J. Choi, Energy method for selection of degrees of freedom in condensation, AIAA J. 38 (7) (2000) 1253–1259.
[22] M. Cho, H. Kim, Element-based node selection method for reduction of eigenvalue problems, AIAA J. 42 (8) (2004) 1677–1684.
[23] A. Ibrahimbegovic, E.L. Wilson, Automated truncation of Ritz vector basis in modal transformation, ASCE J. Eng. Mech. Div. 116 (1990) 2506–2520.
[24] D. Markovic, K.C. Park, A. Ibrahimbegovic, Reduction of substructural interface degrees of freedom in flexibility-based component mode synthesis, Internat. J. Numer. Methods Engrg. 70 (2007) 163–180.
[25] K.C. Park, J.G. Kim, P.S. Lee, A mode selection criterion based on flexibility approach in component mode synthesis. in: Proceeding 53th AIAA/ASME/ASCE/AHS /ASC Structures, Structural Dynamics, and Materials Conference USA, Hawaii, 2012.
[26] T.J.R. Hughes, The Finite Element Method: Linear Static and Dynamic Finite Element Analysis, Dover: Mineola, NY, USA, 2000.
[27] M.J. Turner, R.W. Clough, H.C. Martin, L.J. Topp, Stiffness and deflection analysis of complex structures, J. Aeronaut. Sci. 23 (1956) 805–823.
[28] J.G. Kim, G.H. Lee, P.S. Lee, Estimating relative eigenvalue errors in the Craig-Bampton method, Comput. Struct. 139 (2014) 54–64.
[29] E.N. Dvorkin, K.J. Bathe, A continuum mechanics based four-node shell element for general nonlinear analysis, Eng. Comput. 1 (1) (1984) 77–88.
[30] K.J. Bathe, E.N. Dvorkin, A formulation of general shell elements-the use of mixed interpolation of tensorial components, Internat. J. Numer. Methods Engrg. 22 (3) (1986) 697–722.
[31] P.S. Lee, K.J. Bathe, The quadratic MITC plate and MITC shell elements in plate bending, Adv. Eng. Softw. 41 (5) (2010) 712–728.
[32] K.J. Bathe, P.S. Lee, Measuring the convergence behavior of shell analysis schemes, Comput. Struct. 89 (3–4) (2011) 285–301.
[33] Y.G. Lee, K. Yoon, P.S. Lee, Improving the MITC3 shell finite element by using the Hellinger–Reissner principle, Comput. Struct. 110–111 (2012) 93–106.
[34] R.B. Lehoucq, D.C. Sorensen, C. Yang, ARPACK Users' Guide: solution of large scale eigenvalue problems with implicitly restarted Arnoldi methods, Software Environ, 1997.
[35] A. Ibrahimbegovic, H.C. Chen, E.L. Wilson, R.L. Taylor, Ritz method for dynamic analysis of linear systems with non-proportional damping, Int. J. Earthq. Eng. Struct. Dyn. 19 (1990) 877–889.